ELSEVIER

Ceramics International 32 (2006) 313–319

CERAMICS INTERNATIONAL

www.elsevier.com/locate/ceramint

Effects of resin and graphite content on density and oxidation behavior of MgO-C refractory bricks

B. Hashemi, Z.A. Nemati *, M.A. Faghihi-Sani

Department of Materials Science and Engineering, Sharif University of Technology, Tehran 11365-9466, Iran

Received 21 June 2004; received in revised form 9 December 2004; accepted 4 March 2005
Available online 13 June 2005

Abstract

The effects of resin type and content as well as graphite content on physical and mechanical properties of MgO-C refractories, such as density, porosity and strength were studied. The samples were formulated with various amounts of graphite and resin, and their oxidation behavior was isothermally investigated using a thermo gravimeter (TG), in air and at a temperature ranges from 900 to 1300 °C. The results indicated that, low-viscosity resins improved compressibility, but it degraded the strength. Higher resin content also improved the compressibility, but it caused higher porosity after preheating at 600 °C. The results also showed that the porosity and density of tempered samples were decreased when graphite content were increased. During oxidation process, the rate of weight loss was high at the beginning, but it was gradually decreased when the thickness of decarbonized layer increased. Higher graphite content increased the weight loss, but it would reduce the thickness of oxidized layer.

Keywords: MgO-C refractories; Oxidation; Weight loss; Graphite content; Resin

1. Introduction

In the recent years, MgO-C refractories have been used widely in the steel making industries such as BOF and EAF, because of their high refractoriness and excellent thermal shock and corrosion resistances, resulting from high thermal conductivity, low thermal expansion and low wetability of graphite and high refractoriness of MgO [1]. In this regard, many works have been done. Lubaba et al. [2,3] have investigated the influences of binder type, as well as graphite and MgO particle size distributions on porosity of MgO-C refractories. Tanaka and Kitai [4] has studied relations of physical and mechanical properties of the MgO-C refractories with the particle size distribution and maximum grain size of MgO. Troell and Michael [5] have studied the effects of magnesia and graphite purity on refractoriness, corrosion and oxidation resistances of MgO-C bricks. The effects of resin type were investigated by other research groups [6–8].

Despite the above mentioned advantages, graphite's oxidation is the main drawback of MgO-C refractories, which results in increase of porosity and decrease of strength and corrosion resistance of brick. Some authors have investigated direct and indirect oxidation of graphite in MgO-C refractories [9–11]. Direct oxidation (reaction of graphite with O_2) is the main mechanism at temperatures lower than 1400 °C, but at higher temperatures, the indirect oxidation (reaction of graphite with MgO and formation of dense layer) becomes the main mechanism.

In this research, the effects of graphite content (5–20 wt.%) as well as type and amount of resin, on porosity, density and direct oxidation behavior of MgO-C samples were investigated.

2. Experimental procedure

Cylindrical samples, 30 mm in diameter and 25 mm in height, were prepared using Chinese sintered magnesia (with a purity of 97% and density of 3.5 g/cm^3) and Chinese natural graphite flakes (with an ash content of 5 wt.% and

* Corresponding author. Tel.: +98 21 6165223; fax: +98 21 6012983.
E-mail address: nemati@sharif.edu (Z.A. Nemati).

0272-8842/$30.00
doi:10.1016/j.ceramint.2005.03.008

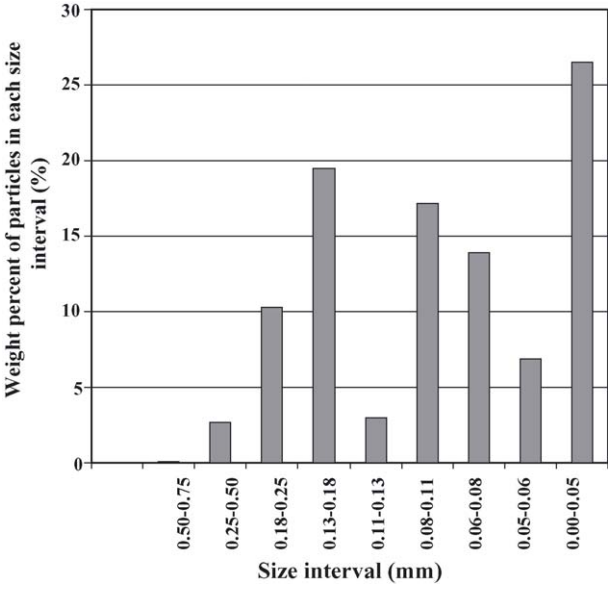

Fig. 1. Particle size distribution of graphite powder.

density of 2.26 g/cm^3). Three types of resin, used in this study, were Novalac A, Novalac B and Resol with the same density of 1.21 g/cm^3 and with different viscosities of 14.5, 10.5 and 6 Pa s, respectively. The MgO particle size distribution was defined according to the Andresen's Equation [$y = 100(d/D)^n$], where n was taken to be 0.5, and four different used particle size ranges were chosen to be 3–5 mm, 2–3 mm, 0.1–2 mm and less than 0.1 mm. Particle size distribution of graphite is presented in Fig. 1.

Samples were carefully mixed, unidirectionally pressed at 120 MPa, and finally tempered at 120 °C or 240 °C (depending on the resin type) for 18 h. Before oxidation tests, the samples were preheated at 600 °C for 5 h in a coke bed, to remove the volatile species of resin. Bulk density and porosity of samples, as well as their cold crushing strength (CCS) were measured before and after preheating, according to ASTM C 373-88 (1999) and ASTM C 773-88 (1999) standard tests, respectively.

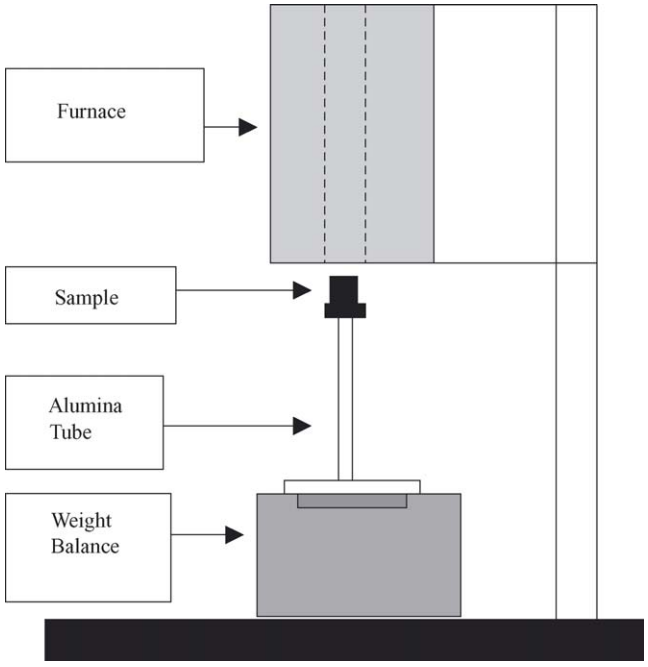

Fig. 2. Schematic view of setup, used for weight loss measurement.

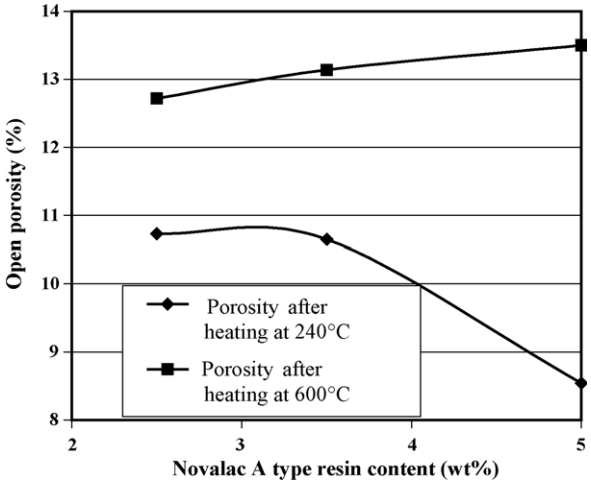

Fig. 3. Open porosity changes vs. Novalac A type resin content.

Isothermal oxidation tests were carried out at various temperatures (900, 1100 and 1300 °C) using a thermo gravimeter (TG) and the results were plotted as weight loss versus time. Fig. 2 shows the experimental apparatus, used for the oxidation test. Inside diameter of the tubular furnace was 45 mm, and a natural convection of air was permitted inside the furnace during the test. The two ends of sample were covered by alumina plates to permit only the straight side of cylindrical sample to be oxidized. The furnace was first heated to the desired temperature, and then each sample was inserted inside it within 2–3 min. During the test, weight loss was recorded at a regular interval of oxidation time.

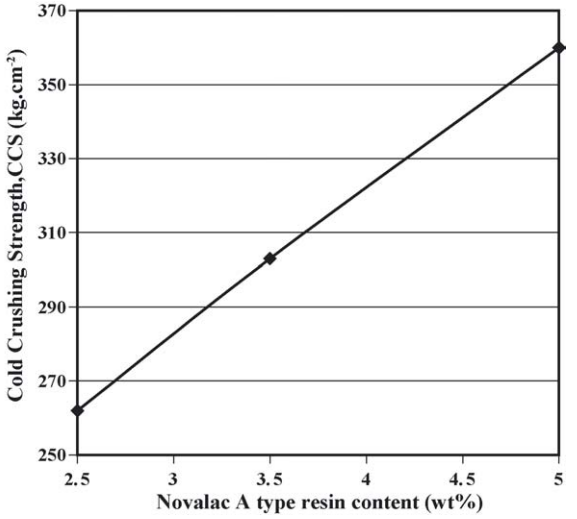

Fig. 4. Cold crushing strength of the tempered samples vs. Novalac A type resin content.

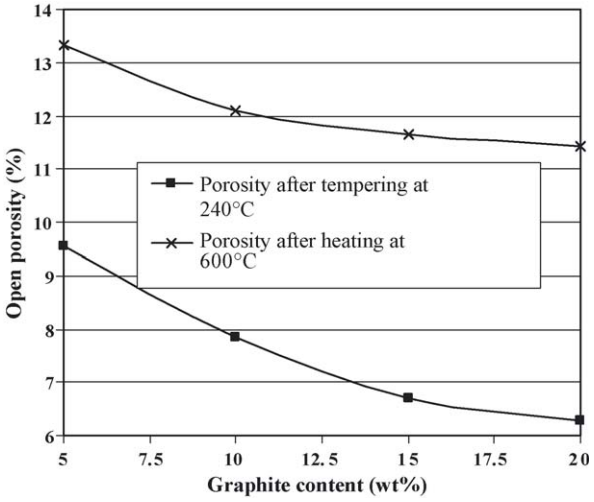

Fig. 5. Changes of open porosity vs. graphite content.

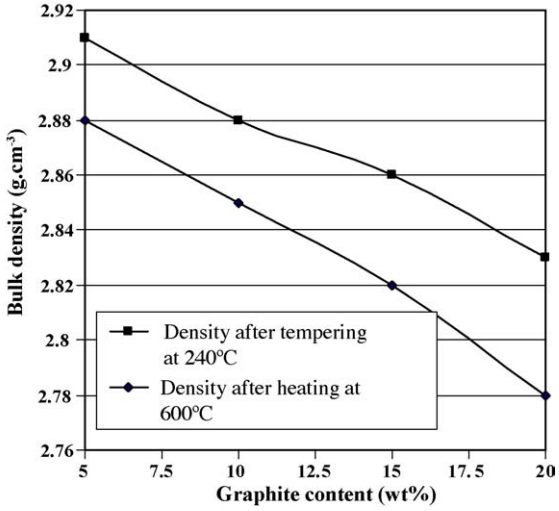

Fig. 6. Changes of bulk density vs. graphite content.

3. Results and discussion

Open porosity changes of samples versus their resin content (Novalac A type) have been plotted in Fig. 3. In the tempered samples, porosity decreased when the resin content increased. This effect might be due to the improvement of compaction during pressing and occupation of pores, as resin content increased. But, in the preheated samples at 600 °C, the porosity increased when the resin content increased, which is believed to be resulted from burning out of total organic portion of resin (about 70 wt.%). Higher resin content causes higher value of burn-out or weight loss, and therefore higher porosity. On the other hand, as Fig. 4 shows, cold crushing strength of the tempered samples increased when their resin content increased, due to decrease of porosity and improvement of resin bonds.

Properties of samples containing different types of resin have been given in Table 1. Sample containing Novalac A presents lower density, because of its higher viscosity and therefore lower compressibility. In comparing with Novalac B, sample containing Resol has almost the same or a little smaller density after tempering, but it has higher density after preheating at 600 °C. As indicated in Table 1, Resol has higher carbon residue after preheating at 600 °C (lower total weight loss), even though it releases larger amount of volatile species during tempering. Lower viscosity of Resol also improves compressibility of sample. As a result, after heating at 600 °C, the sample containing Resol has the highest density.

The effects of graphite content on open porosity and bulk density have been shown in Figs. 5 and 6, respectively. Increase in graphite content improved the compaction during pressing and therefore decreased the porosity. The bulk density decreased due to lower density of graphite, in comparing with magnesia. These results are in a good agreement with results of others such as Lubaba et al. [2,3]. Lower slope of open porosity-graphite content curve for the preheated samples at 600 °C in Fig. 5 (in comparing with the tempered samples) must be due to irreversible expansion of graphite during preheating. More graphite content causes more irreversible expansion. This phenomenon can also explain the higher slope of bulk density-graphite content curve for the preheated samples at 600 °C in Fig. 6 (in comparing with the tempered samples). Since all samples were preheated at 600 °C before oxidation test, porosity and density of only preheated samples must be considered to discuss their oxidation behavior, while compaction behavior of the samples can be understood by comparing the porosity changes in the tempered samples.

One of the most precise and comparable method of presenting the oxidation behavior is based on the changes of oxidized layer thickness versus oxidation time. This method can be used by studying the cross section of each oxidized sample at various specified oxidation times and direct measurement of oxidized layer thickness. As it is shown in Fig. 7, the oxidized and unoxidized regions are clearly separated with an interface, which moves inward as oxidation proceeds.

Table 1
Weight loss, porosity, density and CCS of samples containing 5 wt.% of different resin types

Resin type	Resin weight loss (wt.%)			Open porosity (%)		Bulk density (g/cm^3)		CCS after tempering (kg/cm^2)
	After tempering	After preheating	Total	After tempering	After preheating	After tempering	After preheating	
Novalac A	40	30	70	8.45	13.5	2.77	2.72	360
Novalac B	39	34	73	6.87	11.97	2.82	2.77	320
Resol	41	19	60	8.55	11.15	2.81	2.79	250

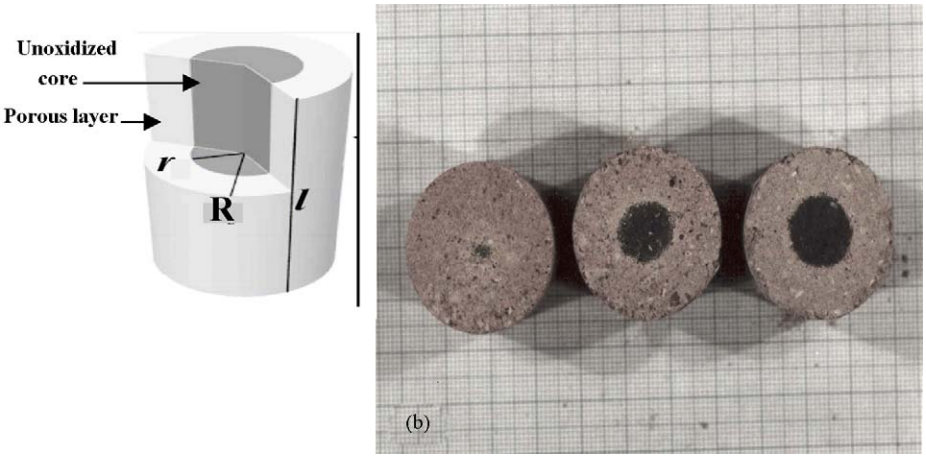

Fig. 7. (a) Schematic view of oxidized sample and (b) cross section of samples after oxidation at different temperatures.

Moreover, the thickness of oxidized layer ($R - r$) at each oxidation time can be mathematically calculated according to the TG experimental results and the following equations (referring to the Fig. 7a):

$$X = 1 - \left(\frac{r}{R}\right)^2 \quad \text{or} \quad R - r = R[1 - (1 - X)]^{0.5} \qquad (1)$$

In which, X is the fraction of weight loss (based on the initial graphite content) at each oxidation time, r is radius of unoxidized region at each oxidation time, and R is initial radius of sample. Table 2 presents direct measurement (experimental) and mathematical calculation results of the oxidized layer thickness at various given oxidation times. As these results show, the experimental and calculated results are almost the same.

Oxidation test results of samples with various graphite contents at 1100 °C have been presented in Fig. 8, as percent of weight loss (based on the initial total weight of sample) versus time. As it is shown, at a given oxidation time, the weight loss increases when graphite content increases. Moreover, in the all samples, the rate of weight loss decreases as oxidation proceeds.

Considering the fact that in the cylindrical samples the surface area of oxidation reaction interface decreases with oxidation time (Fig. 7), the oxidation rate at each oxidation time was calculated based on weight loss per the surface area of reaction interface per time, and presented in Fig. 9. The surface area of reaction interface at a given oxidation time was also calculated based on the radius of unreacted core (r) in Eq. (1) and the related value of weight loss. As Fig. 9 shows, the oxidation rate is high at the beginning, but it decreases as oxidation process goes on. In fact, in the early stage of oxidation, the overall oxidation rate is controlled by the chemical reaction rate on the surface of sample. As oxidation proceeds, a porous oxidized layer gradually forms near the surface, and the reaction interface moves inward. In this condition, gaseous oxygen must diffuse through this layer to reach the reaction interface. Therefore, the oxidation rate decreases.

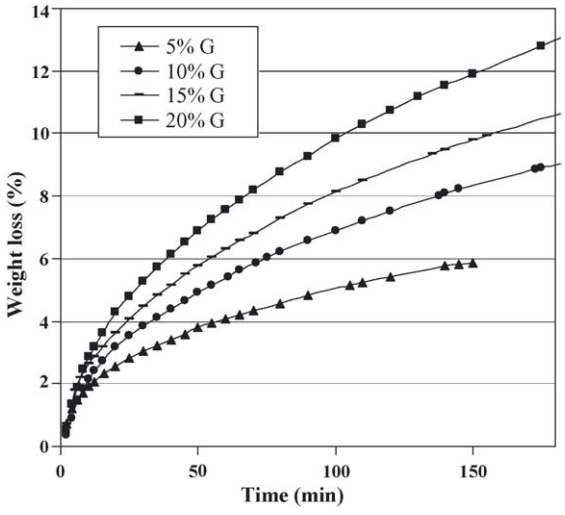

Fig. 8. Weight changes of samples including various graphite contents vs. oxidation time at 1100 °C.

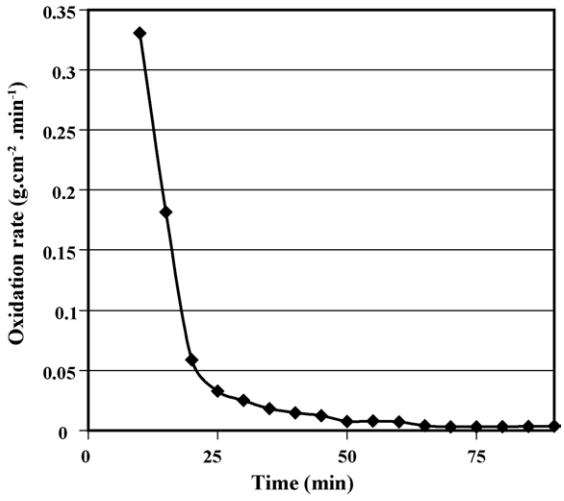

Fig. 9. Oxidation rate (weight loss per reaction surface area per oxidation time) of sample, containing 15 wt.% G, at 1100 °C.

Table 2
Thickness of oxidized layer of some samples after oxidation tests

Sample	Percent of graphite	Temperature of test (°C)	Oxidation time (min)	Calculated oxidized layer thickness (mm)	Measured oxidized layer thickness (mm)	Percent of error
1	20	1100	230	10.6	10.5	0.95
2	20	900	165	7.0	7.4	5.41
3	15	1100	70	5.2	5.0	4.0
4	15	900	90	5.3	5.1	3.92
5	10	1100	190	9.7	9.5	2.11
6	10	900	190	8.7	8.5	2.35
7	10	800	165	7.1	7.0	1.43

The effect of oxidation temperature on the oxidation behavior of samples containing 10 wt.% graphite is shown in Fig. 10. As shown in this figure, when the oxidation temperature rises, the oxidation rate increases which is believed to be resulted from increasing of the chemical reaction rate constant (k_c) and the effective diffusion coefficient (D_e). This figure also shows that the oxidation rate increases more rapidly at higher temperatures. The oxidation curves at 900 and 1100 °C are closed to each other, but both are far from the oxidation curve at 1300 °C. Exponentially dependence of D_e and k_c to temperature can explain these results.

Fig. 11 presents changes of oxidized layer thickness versus oxidation time at 1100 °C for the samples containing various graphite contents. The oxidized layer thicknesses were calculated based on Eq. (1) and the experimental data in Fig. 8, as mentioned before. As can be seen clearly, the thickness of oxidized layer decreases when graphite content increases. It seems that, this result is in contradictory to the previous result in Fig. 8. To explain these contradictory results, it is necessary to consider both effective diffusion coefficient (D_e), which mainly depends on the oxidized layer porosity, as well as inward moving rate of reaction interface, which mainly depends on volume fraction of graphite in the sample. For the former consideration, D_e can be calculated according to Eq. (2) [11], with the assumption that the oxidation is a diffusion control process [12,13].

$$t = A[X + (1 - X)\ln(1 - X)]; \quad A = \left(\frac{\boldsymbol{\rho}_{mG} R^2}{8 C_{O_2} D_e}\right) \tag{2}$$

In these equations, t is the oxidation time, X is fractional weight loss, $\boldsymbol{\rho}_{mG}$ is molar density of graphite in the sample, R is initial radius of sample, C_{O_2} is the concentration of O_2 near the surface of sample and D_e is effective diffusion coefficient through the oxidized layer.

In this regard, value of the term $[X + (1 - X)\ln(1 - X)]$ was calculated at each oxidation time, according to the oxidation test results in Fig. 8. Then, the constant parameter A and consequently D_e were determined by adopting a linear regression method, based on Eq. (2), on the obtained results (values of time versus values of $[X + (1 - X)\ln(1 - X)]$). Linear changes of $\ln(D_e)$ with $1/T$ in Fig. 12 indicates the expected Arrhenius type relationship of the calculated diffusion coefficient with temperature. Fig. 13 also shows the diffusion coefficient of samples containing various graphite contents at 900 and 1300 °C. The obtained D_e values in this work are closed to Li et al. results [14], but they are half of Faghihi-Sani and Yamaguchi results [13]. According to these data, the diffusion coefficient increases

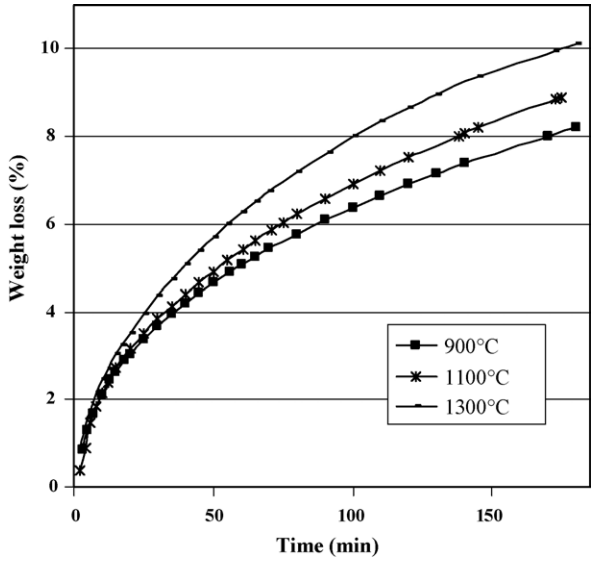

Fig. 10. Weight loss of samples (10 wt.% G) at various temperatures vs. oxidation time.

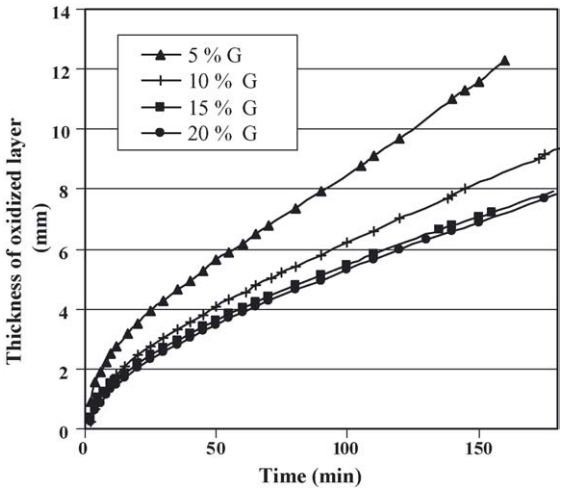

Fig. 11. Changes of oxidized layer thickness of samples, including various graphite contents, at 1100 °C.

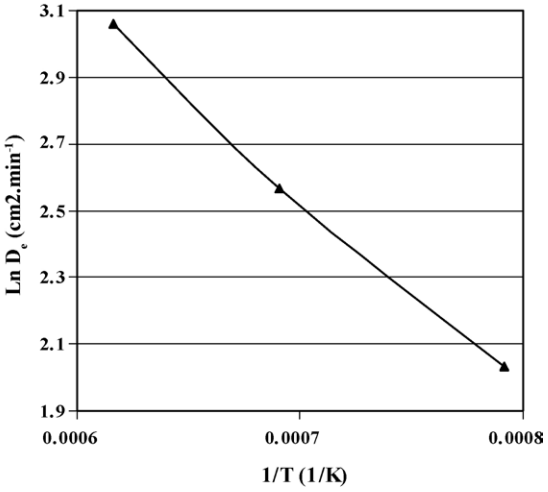

Fig. 12. Arrhenius plot of D_e vs. T for samples containing 10 wt.% G.

when graphite content increases, which is due to increase of porosity in oxidized layer. This effect is partially retarded resulting from decreasing effect of graphite content on initial porosity of the samples (before oxidation), as mentioned in Fig. 5.

To explain the contradictory results in Figs. 8 and 11, simultaneous effects of D_e and $\boldsymbol{\rho}_{mG}$ on oxidized layer thickness have been considered in Eq. (3), which was obtained through combination of Eqs. (1) and (2).

$$t = A\left[1 - \left(\frac{r}{R}\right)^2 + 2\left(\frac{r}{R}\right)^2 \ln\left(\frac{r}{R}\right)^2\right] \quad \text{or} \quad t = A\,f(r) \tag{3}$$

For a given oxidized layer thickness $(R - r)$ or r, oxidation time ratio of a sample containing X wt.% graphite to the sample containing 5 wt.% graphite can be presented

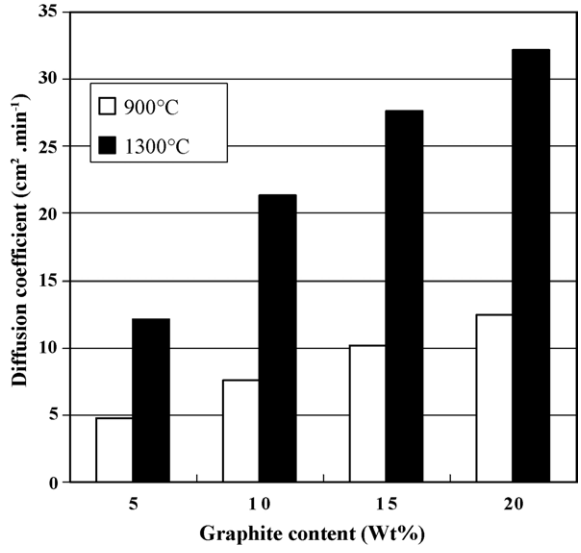

Fig. 13. Diffusion coefficient changes vs. graphite content.

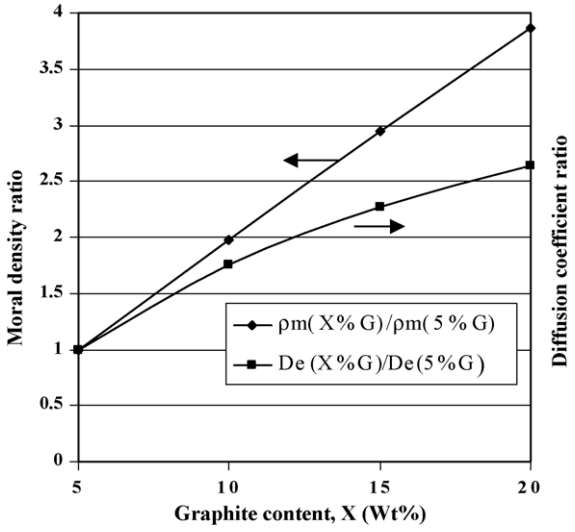

Fig. 14. Changes of graphite molar density ratio and effective diffusion coefficient ratio at 1300 °C vs. graphite content.

by Eq. (4).

$$\frac{t_{X\%G}}{t_{5\%G}} = \left[\frac{\boldsymbol{\rho}_{mG(X\%G)}/\boldsymbol{\rho}_{mG(5\%G)}}{D_{e(X\%G)}/D_{e(5\%G)}}\right] \tag{4}$$

Variations of $(\boldsymbol{\rho}_{mG(X\%G)}/\boldsymbol{\rho}_{mG(5\%G)})$ and $(D_{e(X\%G)}/D_{e(5\%G)})$ versus graphite content (X%G) have been shown in Fig. 14. As it seems, both ratios increase when graphite content increases. However, increasing rate of molar density ratio is higher than that of effective diffusion coefficient ratio. Therefore, oxidation time ratio increases with increase in graphite content. In other word, to form the same oxidized layer thickness, longer oxidation time is required for samples with higher graphite content.

Although thickness of oxidized layer decreases with increase in graphite content, its porosity increases. This may result in degradation of strength and corrosion resistance. Therefore, optimum graphite content must be selected to meet the desired properties in the system.

4. Conclusion

Increase in resin content improved compressibility during pressing and consequently increased the CCS of the tempered samples. Among various resin types, samples containing Resol had the lowest porosity after heating at high temperature, resulting from its lower viscosity and lower content of volatile species.

Increase in graphite content improved compressibility during pressing and therefore decreased the porosity. However, this effect was diminished, due to the irreversible expansion of graphite at higher temperatures.

Calculation of the oxidized layer thickness changes with oxidation time, based on the weight loss results of TG test

and the proposed equations, showed that with increase in graphite content, the thickness of oxidized layer decreased even if the weight loss increased. These results were successfully explained by determining changes of the effective diffusion coefficient as well as the graphite molar density with the changes of graphite content.

References

[1] S. Banerjee, Recent developments in steel-making refractories, in: Proceedings of the Unified International Technical Conference on Refractories, Mexico, 2001, pp. 1033–1041.
[2] N.C. Lubaba, B. Rand, N.H. Brett, Effect of carbon binders on the development of porosity in MgO-C composite refractories, Br. Ceram. Trans. J. 87 (1988) 164–167.
[3] N.C. Lubaba, B. Rand, N.H. Brett, Compaction studies of MgO-Flake graphite mixtures relevant to the fabrication of composite refractory materials, Br. Ceram. Trans. J. 87 (1988) 158–163.
[4] M. Tanaka, T. Kitai, The influence of magnesia particle size distribution on the physical properties of MgO-C bricks, in: Proceedings of the Unified International Technical Conference on Refractories, Japan, 1995, p. 116.
[5] P.T. Troell, O.J. Michael, Advances in the development and application of magnesia-carbon bricks, in: Proceedings of the Unified International Technical Conference on Refractories, Aachen, 1991, p. 247.
[6] D. Nishimura, Technical trends of phenolics for Japanese refractories, Taikabutsu Overseas 15 (2) (1995) 10–14.
[7] C.G. Aneziris, D. Borzov, Resin-bonded magnesia-carbon refractories with cal-tar resin additive for steel industry, Cfi/Ber. DKG 80 (5) (2003) E1–E4.
[8] K. Kanno, N. Koike, Y. Korai, Mesophase pitch and phenolic resin blends as binder for magnesia graphite bricks, Carbon 37 (1999) 195–201.
[9] K. Anan, Wear of refractories in basic oxygen furnaces (BOF), Taikabutsu Overseas 21 (4) (2001) 241–246.
[10] A. Yamaguchi, Control of oxidation-reduction in MgO-C refractories, Taikabutsu Overseas 4 (1) (1984) 32–36.
[11] R.W. Missen, C.A. Mims, Introduction to Chemical Reaction Engineering and Kinetics, John Wiley & Sons Inc., New York, 1999,p. 224.
[12] N.K. Ghosh, D.N. Ghosh, K.P. Jagannathan, Oxidation mechanism of MgO-C in air at various temperatures, Br. Ceram. Trans. J. 99 (3) (2000) 124–129.
[13] M.A. Faghihi-Sani, A. Yamaguchi, Oxidation kinetics of MgO-C refractory bricks, Ceram. Int. 28 (2002) 835–839.
[14] X. Li, M. Rigaud, S. Palco, Oxidation kinetics of graphite phase in magnesia-carbon refractories, J. Am. Ceram. Soc. 78 (4) (1995) 965–971.